# Journal of Materials Chemistry A

Accepted Manuscript


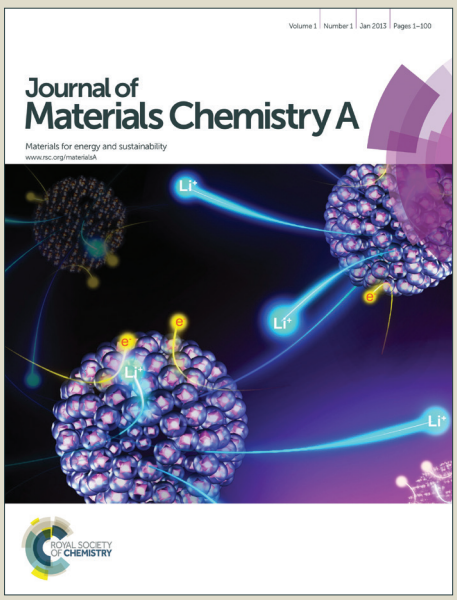





ROYAL SOCIETY OF CHEMISTRY

www.rsc.org/materialsA

Journal of Materials Chemistry A

Cite this: DOI: 10.1039/c0xx00000x

www.rsc.org/xxxxxx

Paper

# Plasmonic, Interior-decorated, One-dimensional Hierarchical Nanotubes for High-efficiency, Solid-state, Dye-sensitized Solar Cells

**Sung Hoon Ahn, Dong Jun Kim, Won Seok Chi, Jong Hak Kim***

**Received (in XXX, XXX) Xth XXXXXXXXX 20XX, Accepted Xth XXXXXXXXX 20XX**
**DOI: 10.1039/b000000x**

We report a high energy conversion efficiency of 8.4% at 100 mW $cm^{-2}$, which is one of the highest values for N719-based, solid-state, dye-sensitized solar cells (ssDSSCs). Our solar cells are based on one-dimensional (1D) hierarchical hetero-nanotubes consisting of Au cores and $SnO_2/TiO_2$ nanosheet double shells (referred to as Au@$SnO_2$@TNS). Carbonaceous nanofibers (CNFs) with tellurium (Te) cores are used as dual templates for the inner-deposition of gold and the outer-deposition of the metal oxides layer. An organized mesoporous $TiO_2$ (OM-T) film, with high porosity, large pores, and good interconnectivity, is also prepared via a graft copolymer template approach and utilized as a matrix to disperse the 1D hierarchical nanostructures. Such nanostructures provide good pore-filling for solid electrolytes, faster electron transfer, and enhanced light scattering, as confirmed by reflectance spectroscopy, incident photon-to-electron conversion efficiency (IPCE), and intensity-modulated photocurrent spectroscopy (IMPS)/intensity-modulated photovoltage spectroscopy (IMVS).

## Introduction

Dye-sensitized solar cells (DSSCs) are promising solar devices due to their low cost, easy fabrication, and relatively high efficiency (~12 %) as compared to conventional silicon-based solar cells[1]. DSSCs are typically fabricated by depositing a dye-adsorbed $TiO_2$ film on a transparent conductive oxide (TCO) substrate as the photoanode, which is then combined with a redox iodide/triiodide redox electrolyte couple and a Pt-coated TCO substrate as the counter electrode. Considerable efforts have been made to improve their cell efficiency and stability by using functional photoanode materials,[2-5] novel sensitizers with large absorption coefficients,[6] and an efficient redox electrolyte.[7,8] Despite the high energy conversion efficiency of DSSCs with an $I^-/I_3^-$ liquid electrolyte, solid-state DSSCs (ssDSSCs) have recently received much attention due to the need for long-term stability, flexible design, and lightweight cells. Several approaches have been reported for ssDSSCs based on a solid electrolyte but most of the reported efficiencies have been below 8%, which is much lower than the efficiencies of their counterparts using a liquid electrolyte.[7-11] We report a high energy conversion efficiency of 8.4% at 100 mW $cm^{-2}$, which is one of the highest values for ssDSSCs with an N719 dye.[7-11] Our process is based on one-dimensional (1D) hierarchical hetero-nanotubes consisting of a Au cores and $SnO_2/TiO_2$ nanosheet double shells, referred to as Au@$SnO_2$@TNS.

In photon-to-electricity devices using solar light as the energy source (e.g., DSSCs), the energy conversion efficiency from photons to electricity can be improved in two ways. First, maximizing the light harvesting efficiency is related to absorbing as much of the spectrum of solar light as possible. Second, the absorbed solar energy must be converted to electricity in a way that minimizes energy losses. In terms of light harvesting, tremendous efforts have been devoted to a variety of techniques including extending the acceptable solar spectrum by developing new sensitizers that can absorb a wide spectrum of solar light including near infrared region. Additionally, perovskite solar cells have recently been developed with a high efficiency over 15% due to their strong light absorption and greater than one-micrometer charge diffusion length when combined with spiro-MeOTAD (2,2′,7,7′-tetrakis(N,Ndi-p-methoxyphenyl-amine)-9,9′-spirobifluorene) as the hole conductor.[12] Another approach to increase light harvesting is to utilize the absorbed solar light efficiently and trap light inside the solar cell. For this purpose, nanoparticles with various functionalities have been incorporated into the $TiO_2$ photoanode, including large-sized scattering nanoparticles[13] to increase the photon path length, plasmonic metal nanoparticles to induce surface plasmon resonance,[14-17] or up-converting nanoparticles that can convert near-infrared photons into visible-light.[18-20] Also, engineering the nanostructure of the photoanode by including nano/micro patterning,[21-24] photonic crystals,[25-27] and layer-by-layer Bragg stack[28-30] structures could intensify and scatter a specific light spectrum.

Among these techniques, the incorporation of plasmonic noble metal nanoparticles has been intensely studied due to their several advantages in photo-electrical conversion devices. Most studies have focused on the enhancement of light absorption and trapping by plasmonic nanoparticles due to localized surface plasmon resonance. The additional role of plasmonic nanoparticles on the electrochemical properties of DSSCs have also been studied including the negative shift of the Fermi level driven by the electron charging effect,[31,32] enhancement of electron separation and reduced recombination by localized electromagnetic field,[32,33] and reduced binding energy of the light absorber.[16] Typically, plasmonic metal nanoparticles have been mixed with metal oxide photoanodes for DSSCs and combined with various nanostructures to create synergetic effects. However, the exposure of metal nanoparticles to the electrolyte often leads to ineluctable problems such as recombination and back reaction of the charge carriers in addition to thermal and chemical instability due to continuous corrosion caused by the electrolyte and calcination during high temperature annealing for crystallization of the metal oxides. Thus, plasmonic nanoparticles must be protected by a metal oxide shell[32-35] in order to prevent their exposure to the electrolyte. However, the thickness of shell

must be carefully adjusted due to the distance-sensitive electric field dye excitation.[17,33,35] Additionally, direct adsorption or deposition of plasmonic nanoparticles on the surface of $TiO_2$ can often lead to a decreased number of the active sites for dye adsorption.[17]

Previously, our group developed a crack-free, micron-thick, well-organized mesoporous structure by combining a self-assembled graft copolymer, poly(vinyl chloride)-g-poly(oxyethylene methacrylate) (PVC-g-POEM), as a structure directing agent with preformed $TiO_2$ nanocrystals.[36,37] These graft copolymer-templated, well-organized $TiO_2$ films have a higher porosity and a greater surface area, enabling high-efficiency ssDSSCs in which pore-filling of the solid electrolyte is critically important. Despite several advantages of the well-organized $TiO_2$ structure for use as the solid-state electrolyte, additional improvements in DSSC performance are still needed to further increase the electron transport and light scattering capabilities.[38,39] The scattering ability and electron transport were optimized by using a hierarchical, double shell nanostructure consisting of high mobility $SnO_2$ nanotubes and ultra-thin $TiO_2$ nanosheets with a tubular outer-shell structure[38] and a hollow sphere structure.[39] This structure should simultaneously enhance the light harvesting and charge collection efficiencies.

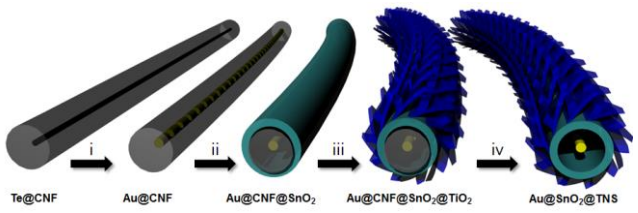


**Fig. 1**. Schematic illustration for the preparation of multifunctional hetero-nanotubes consisting of Au cores and $SnO_2$@$TiO_2$ nanosheet double shells (referred to as Au@$SnO_2$@TNS). i) Te nanowire in the carbonaceous nanofiber (CNF) was replaced with Au nanoparticles via a galvanic replacement reaction, ii) a $SnO_2$ thin layer was coated on the surface of CNF, iii) ultra-thin $TiO_2$ nanosheets (TNSs) were deposited on the surface of the $SnO_2$ layer via a hydrothermal reaction, and iv) CNF was selectively removed and the metal oxides were crystallized by high temperature annealing at 450 $^oC$ for 30 min.

In this study, we developed a more effective photoanode using the synergetic effects of inner-decorated, aligned plasmonic nanoparticles along a hierarchical, 1D metal oxide nanotube structure. The synergetic effect of the inner-decorated, aligned plasmonic nanoparticles and the well-designed, multifunctional nanostructure in ssDSSCs were characterized in terms of their light harvesting and charge collection properties. The inner-decoration with gold (Au) nanoparticles by a galvanic replacement reaction maximizes the plasmon-induced benefits and simultaneously prevents exposure to the electrolyte, which causes problems associated with carrier recombination and thermal and chemical instability, without the need for any additional protection layer. When 1D hierarchical nanostructures with plasmonic metal cores were incorporated into organized $TiO_2$ films, a high energy conversion efficiency (up to 8.4%) was recorded. This is one of the highest values for an N719 dye-based ssDSSCs. The detailed structural and optical properties of the plasmonic 1D structures were characterized systematically by field emission-scanning electron microscopy (FE-SEM), energy filtered transmission electron microscopy (EF-TEM), and diffuse reflectance spectra. The ssDSSCs were fabricated using a solid-state polymerized ionic liquid, and their performance was characterized using current-voltage (J–V) curves, incident photon to current conversion efficiency (IPCE) spectra, and intensity-modulated photocurrent spectroscopy (IMPS) / intensity-modulated photovoltage spectroscopy (IMVS).

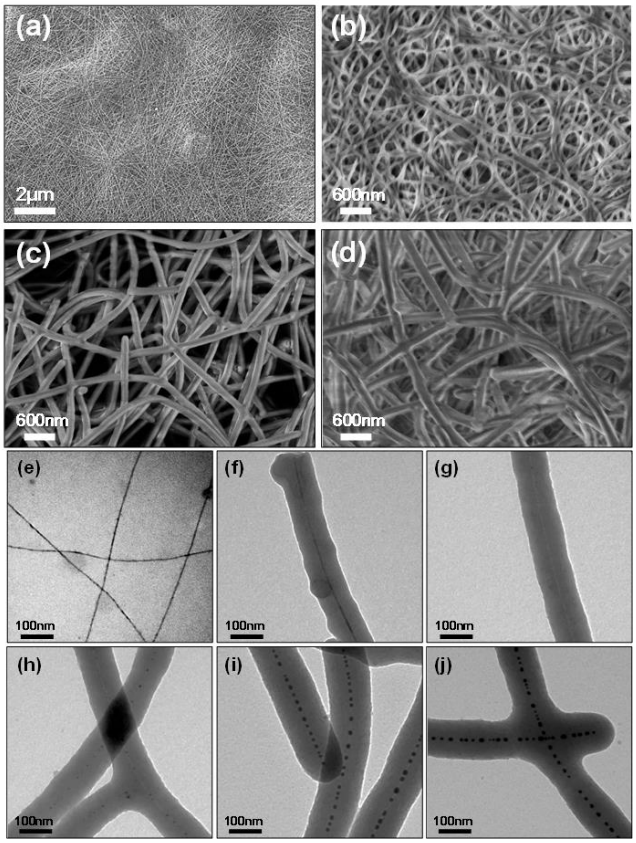


**Fig. 2**. FE-SEM images of (a) Te nanowires. FE-SEM images of Te@CNF after hydrothermal reaction at 160 $^oC$ for (b) 18 h, (c) 36 h, and (d) 48 h. The diameter of each one-dimensional structure is (a) 5~6 nm, (b) 40~50 nm, (c) 90~100 nm, (d) 140~150 nm. EF-TEM images of (e) Te nanowires, (f) Te@CNF, (g) etched pure CNF, (h) Au1@CNF, (i) Au2@CNF, and (j) Au3@CNF after a galvanic exchange reaction.

## Results and Discussion

Multifunctional, hierarchical, 1D hetero-nanotubes consisting of Au cores and $SnO_2$@$TiO_2$ double shells were prepared, as illustrated in **Fig. 1**. First, ultra-thin tellurium (Te) nanowires with a high aspect ratio were prepared via a hydrothermal method using poly(vinyl pyrrolidone) (PVP) as a structure-controlling agent in ethylene glycol (**Fig. 2a)**. The tellurium nanowires were then uniformly coated with a carbonaceous material (e.g., glucose) via a hydrothermal reaction. The use of different reaction times (i.e. 18, 36, and 48 h) at 160 $^oC$ resulted in different diameters of the tellurium@carbonaceous nanofibers (Te@CNFs) (i.e., 50, 100, and 150 nm, respectively) when the other reaction conditions were fixed (**Fig. 2b-d**). It has been reported that the diameter of CNFs can be systematically controlled by the reaction temperature, time, and the ratio of tellurium to the carbonaceous source.[40,41] Furthermore, the diameter of tellurium nanowires can be easily tuned by changing the reaction conditions, providing an effective source, and allowing space for Au exchange. After the hydrothermal reaction in the presence of tellurium nanowires, the precipitated Te@CNFs were filtered and washed thoroughly with water and

ethanol several times. After drying at room temperature overnight, Te@CNFs were dispersed in water by ultrasonication for 1 h to form a wool-like, brown, homogeneous solution.

Prior to the deposition of the metal oxide on the CNF, tellurium cores were exchanged with a gold precursor via a galvanic exchange reaction involving the oxidation of tellurium. This was made possible due to the fact that the ions of gold have a higher reduction potential.[42] Considering the diffusion length for the galvanic exchange reaction from tellurium to gold, as well as the scattering ability of the tubular structure, an intermediate diameter of 100 nm for CNFs with different amounts of gold cores was chosen. Different amounts of gold precursors ($HAuCl_4$) were added to the homogeneous solution at 2, 5, and 10 weight ratios of Au to Te@CNF, which are referred to as Au1@CNF, Au2@CNF, and Au3@CNF, respectively. After deposition of $TiO_2$ nanosheets (TNSs) and selective removal of CNFs, the 1D nanotubular structure, consisting of a gold core and a TNS outer shell, was generated. These samples are referred to as Au1@TNS, Au2@TNS, and Au3@TNS, respectively. To prevent any unintended effects of tellurium doping, the tellurium cores were removed by immersion in an acid $H_2O_2$ solution (HCl : $H_2O_2$ : $H_2O$ = 2 : 5 : 23, v/v) at room temperature for 12 h. After the etching or galvanic replacement reactions, the samples were filtrated and washed. Once tellurium was exchanged with gold, the formation of Te@CNF, etched CNF, and Au@CNF were confirmed by EF-TEM, as shown in **Fig. 2e-j.** The weight ratio of gold to CNF was 0.5, 2, and 4 wt%, respectively, as characterized by energy-dispersive X-ray spectroscopy (EDX) analysis. The tellurium cores could be completely removed (**Fig. 2g)** or exchanged with gold, regardless of the amount of gold precursor (**Fig. 2h-j**).

By considering the plasmonic resonance distance between the gold core and the dye sensitizer adsorbed on the surface of the metal oxide, a relatively thin CNF with a 50 nm diameter (50-CNF) was chosen as the template for $SnO_2$@$TiO_2$ double shells after the gold exchange. A similar exchange reaction with 10 wt% $HAuCl_4$ as the precursor was repeated for 50-CNF. This exchange reaction was confirmed by EF-TEM (**Fig. S1**) and EDX analyses (**Fig. S2).** The galvanic exchange reaction of thick CNF with a 150 nm diameter was rather limited under the same reaction conditions (50 $^oC$ for 12 h), and the size uniformity of the exchanged gold after reaction at a higher reaction temperature (100 $^oC$ for 12 h) was rather poor, as confirmed by TEM images (**Fig. S3)**. For this reason, these samples are excluded from this study.

Hierarchical, bifunctional, ultra-thin $TiO_2$ nanosheets (TNSs) were coated on the surface of plasmonic CNFs to prevent the exposure of gold nanoparticles to the electrolyte using a hydrothermal reaction. Because of the abundant hydroxyl and carbonyl groups on the CNF surface,[43,44] metal oxides can be attached onto the 1D CNF structure with full coverage. The hierarchical nanostructure of the facet-controlled, ultra-thin nanosheets leads to a higher surface area and faster electron transport compared to randomly-organized nanoparticles.[45] The collected pure CNF and Au@CNF were re-dispersed in a 2-propanol, diethylenetriamine (DETA), and titanium(IV) isopropoxide (TTIP) solution by ultrasonication and poured into Teflon-lined autoclaves. This was followed by the hydrothermal reaction at 200 $^oC$ for 24 h. After cooling down naturally, the precipitated products were filtrated and washed.

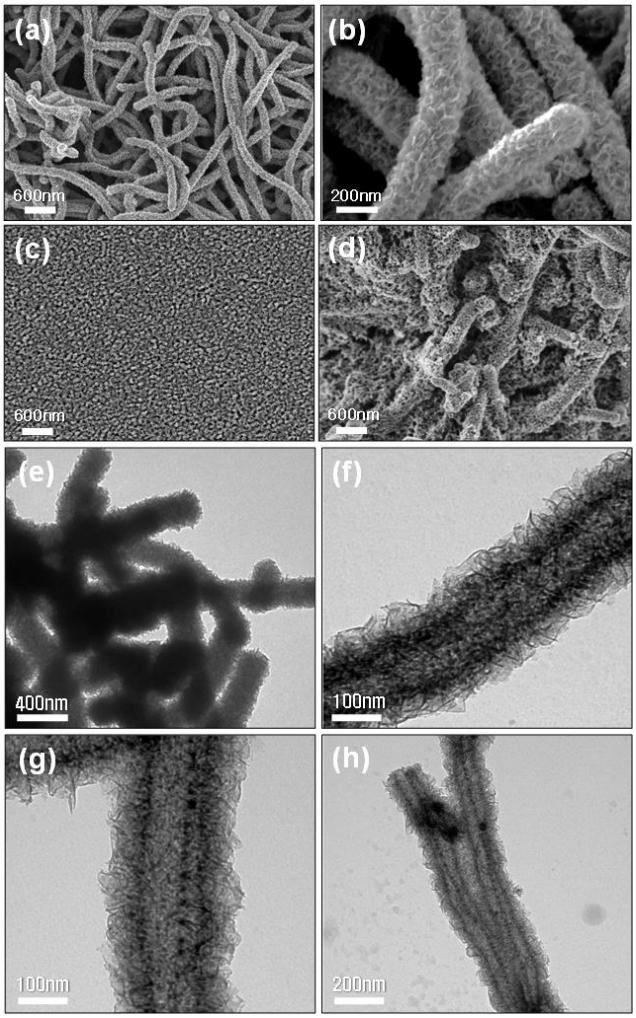


**Fig. 3.** FE-SEM images of (a and b) Au2@TNS, (c) organized mesoporous $TiO_2$ (OM-T) film, and (d) OM-T/Au2@TNS 30% hybrid film. EF-TEM images of CNF@TNS (e) before and (f) after annealing. EF-TEM images of Au2@TNS (g) before and (h) after annealing.

A few layers of TNSs were stacked uniformly on the surface of CNFs, leading to an increase in nanofiber diameter from 100 nm to 150 nm (**Fig. 3a,b**). The morphologies of the hierarchical structure of nanosheet-coated nanotubes were similar, regardless of the amount of the gold core. Multifunctional, plasmonic 1D nanostructures were dried in an oven at 50 $^oC$ overnight and mixed with a structure-directing agent solution containing 10 wt% PVC-g-POEM in tetrahydrofuran (THF) by ultrasonication for 30 min. In order to investigate the structure-property relation, different photoanodes with 10, 15, 20, and 30 weight percent of plasmonic nanostructures (Au2@TNS), relative to the amount of preformed $TiO_2$, were fabricated. In the second group, 20 wt% of Au@TNS with different amounts of gold cores were used to investigate the plasmonic effect, excluding the overlapped enhancement due to the nanostructures. The homogeneous solution was stirred vigorously, followed by the addition of preformed $TiO_2$ nanoparticles, as reported in a previous method.[36-38] Self-assembly of the PVC-g-POEM graft copolymer with the hydrophilically-preformed $TiO_2$ nanocrystals provided an organized mesoporous $TiO_2$ structure (OM-T) with large pore size, high porosity, and good interconnectivity (**Fig. 3c**). The organized mesoporous structure of OM-T was

maintained and homogenized with the plasmonic 1D hetero-nanotubes in the photoanode at 30 wt% loading (**Fig. 3d).** The composite films were cast onto the FTO substrates using the doctor blade technique, followed by annealing at 450 °C for 30 min. The carbonaceous template was completely removed after high temperature annealing, generating the tubular structure with the gold inner-decorated 1D TNS (**Fig. 3e,f**). This unique structure, consisting of inner-aligned gold nanoparticles along the 1D $TiO_2$ nanotubes for Au2@TNS, was confirmed by EF-TEM (**Fig. 3g,h).** Aligning of the gold nanoparticles along the direction of the nanotubes provides an ordered, plasmonic-active pathway, which simultaneously enables fast electron transport and multi-functional plasmonic effects and prevents direct contact between the electrolyte and the noble metal nanoparticles. The effects of 1D TNSs on mesoporous $TiO_2$ films, in terms of surface area and pore size distribution, were characterized by Brunauer-Emmett-Teller (BET) surface area analysis and Barrett-Joyner-Halenda (BJH) measurements, as shown in **Fig. S4** and summarized in **Table 1**. The addition of 1D TNS resulted in an increase in the surface area of OM-$TiO_2$ films, proportional to the amount of ultra-thin nanosheet-based material. Upon the addition of the 1D nanostructure, broad maximum peaks in the pore size distribution curves were found, indicating bimodal porosity, which is effective for simultaneously increasing the surface area and pore-infiltration of the electrolyte.[38,39]

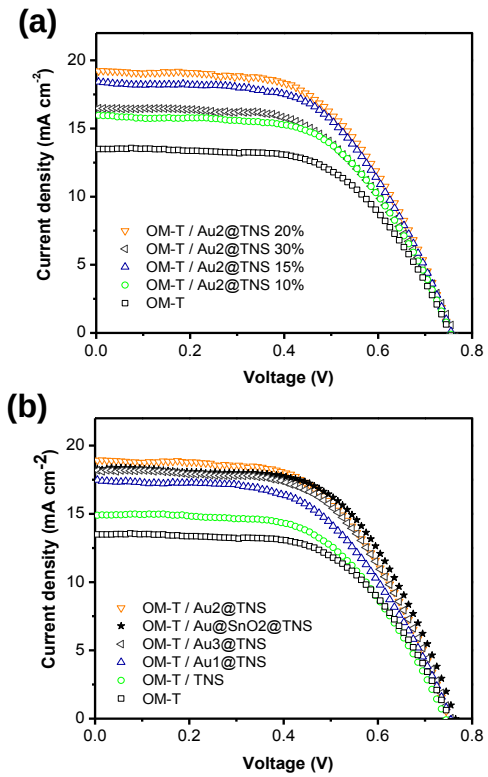


**Fig. 4.** J-V curves of ssDSSCs fabricated with various photoanodes and a solid PEBII electrolyte at 100 mW $cm^{-2}$: (a) organized mesoporous $TiO_2$ (OM-T) where OM-T has different amounts of Au2@ TNS, (b) OM-T/TNS with different amounts of Au cores.

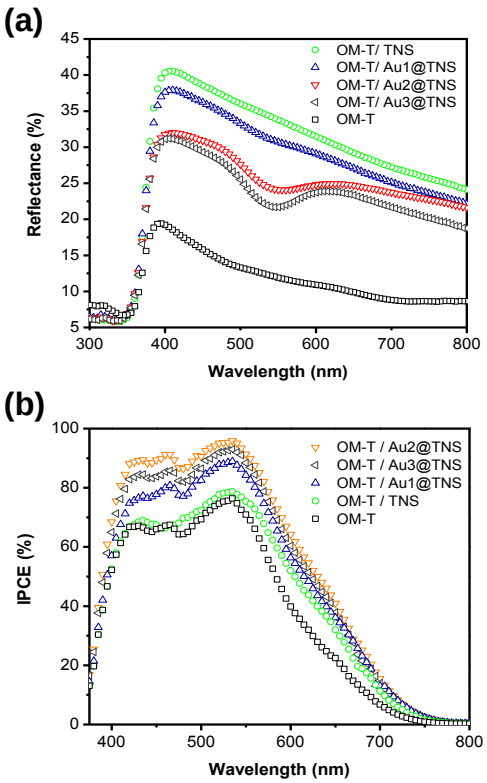


**Fig. 5.** (a) diffuse reflectance spectra of OM-T films with and without Au nanoparticles, and (d) IPCE curves of ssDSSCs at 100 mW $cm^{-2}$.

1D $TiO_2$ nanotubes with and without gold cores were added to the OM-$TiO_2$ matrix and used as the photoanodes in ssDSSCs with a solid electrolyte. Poly((1-(4-ethenylphenyl)methyl)-3-butyl-imidazolium iodide) (PEBII)[36-39] was synthesized through a free radical polymerization reaction and used, without any additives (e.g., iodine ($I_2$) or iodide salt), as the solid electrolyte for ssDSSCs. The high mobility of PEBII arises from the well-ordered molecular structure with π-π stacking interactions and a low glass transition temperature of -4 °C. The OM-T film showed higher photo-to-electricity conversion efficiency compared to a commercial Dyesol paste, which was caused by the improved solar cell parameters including the short-circuit current density ($J_{sc}$), open-circuit voltage ($V_{oc}$), and fill factor (FF). These improved properties are attributed to the larger surface area, higher porosity, and good interconnectivity of the OM-T film, which are essential for solid-state electrolyte infiltration.[46] The optimized weight ratio of Au2@TNS to OM-T was found to be 20 wt%, where the highest efficiency (8.0%) was obtained, as shown in the current density-voltage (J-V) curves in **Fig. 4a and Table 1.** The synergetic effect on the performance enhancement achieved by using OM-T/Au@TNS composite cells is caused by i) excellent scattering ability due to voids in the tubular structure, ii) facile electron transport along the 1D nanostructure, iii) larger surface area due to a well-organized mesoporous structure and ultra-thin nanosheets, and iv) plasmonic properties of the gold nanoparticles. However, despite its greatest surface area (139.7 $m^2/g$), the performance improvement of OM-T/Au2@TNS 30% was offset by the unfavorable effect caused by an excess amount of plasmonic nanocomposites. By incorporating Au2@TNS into the OM-T film, the overall conversion efficiency of ssDSSCs was significantly increased compared to the bare OM-T film. This improvement was mainly due to the enhancement in the $J_{sc}$

(without a loss of $V_{oc}$), indicating that most of the inner-decorated gold nanoparticles in the nanotube structure were successfully blocked from the electrolyte. However, FF values slightly decreased from 0.58 to 0.55~0.56, presumably due to the partial exposure of plasmonic nanoparticles through broken nanotubes.

To systematically elucidate and distinguish the effect of the inner-decorated plasmonic properties alone, the same amount (20 wt%) of Au@TNS containing different amounts of gold cores, controlled by the galvanic replacement reaction, were added to OM-T films. The resulting performance of the ssDSSCs was tested (**Fig. 4b**) and is summarized in **Table 1**. Regardless of the ratio of the gold core and surrounding 1D TNSs, there was an optimized amount of plasmonic nanoparticles in the photoanodes, and the main contribution to the efficiency enhancement comes from an improvement in the $J_{sc}$. Further increasing the amount of gold nanoparticles above the optimum concentration resulted in a decrease in ssDSSC performance (e.g. 7.0% for OM-T/Au2@TNS 30%). This dropoff was caused by excess light trapping and absorption by the gold nanoparticles. Although plasmonic solar cells have been studied,[47,48] their potential for commercial production is low because their back electron transfer of the photo-generated electron is quite fast.[49] It is worth noting that the use of hetero-nanotubular structures consisting of gold cores and $SnO_2$@$TiO_2$ double shells (referred to as OM-T/Au@$SnO_2$@TNS 20%) showed the highest efficiency of 8.4% at 100 mWcm$^{-2}$. This structure also showed an increased FF (up to 0.60) and a higher $V_{oc}$ (up to 0.77-0.78 V). This is attributed to the synergetic effect of the plasmonic properties of the gold core and the high mobility of 1D $SnO_2$, which is perfectly surrounded by ultra-thin $TiO_2$ nanosheets to effectively block exposure to the electrolyte.

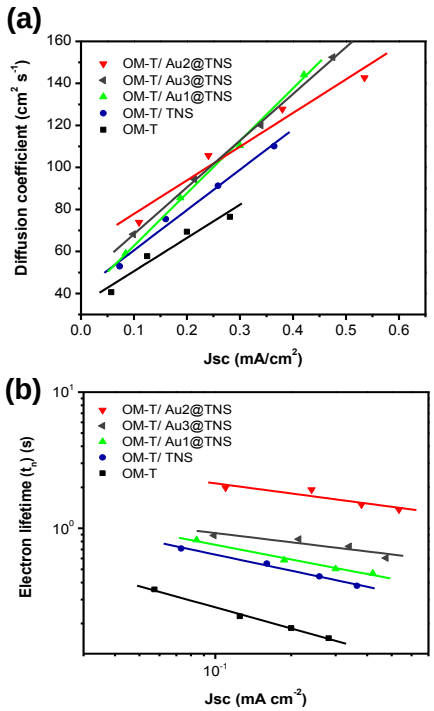


**Fig. 6.** IMPS/IMVS data of ssDSSCs with OM-T, OM-T/TNS, and OM-T/Au@TNS photoanodes and a solid PEBII electrolyte: (a) diffusion coefficient versus $J_{sc}$, (b) electron (recombination) lifetime ($t_n$), (c) diffusion length, and (d) diffusion coefficient versus applied voltage.

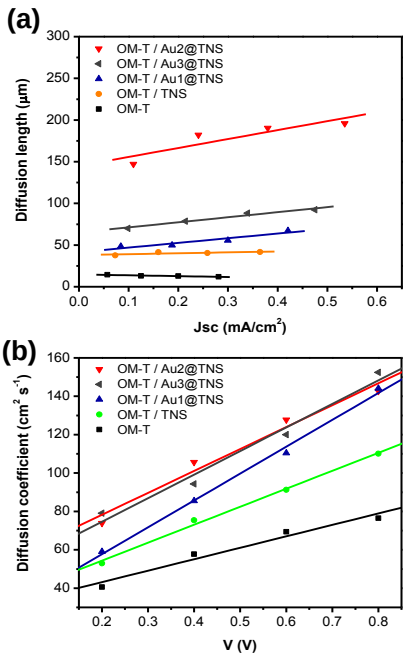


**Fig. 7.** IMPS/IMVS data of ssDSSCs with OM-T, OM-T/TNS, and OM-T/Au@TNS photoanodes and a solid PEBII electrolyte: (a) diffusion coefficient versus $J_{sc}$, (b) electron (recombination) lifetime ($t_n$), (c) diffusion length, and (d) diffusion coefficient versus applied voltage.

In order to investigate the improvement of the optical properties caused by the plasmonic effect, the diffused reflectance UV-vis spectra were measured for OM-T/TNSs containing plasmonic gold cores. This data is shown in **Fig. 5a**. Due to the high transparency of the preformed nanocrystal film (with an ordered mesostructure), the OM-T showed a lower light scattering ability. This can be enhanced by the incorporation of 1D TNSs due to their tubular structure with voids. Interestingly, gold-incorporated photoanodes showed an additional optical absorption region centered at 560 nm. The intensity of this peak is proportional to the amount of gold nanoparticles, which happens to match well with the surface plasma resonance absorption of gold nanoparticles in the $TiO_2$ nanotubes, intensifying the absorption near the plasmonic nanoparticles. As the amount of loaded gold was increased, the overall light reflectance was diminished due to light scattering and absorption inside the nanotubes and film, leading to the trapping of sunlight. A similar tendency for light trapping and additional absorption caused by the plasmonic nanoparticles were observed for plasmonic 1D double shell (Au@$SnO_2$@TNS) hetero-nanotubes consisting of Au cores and $SnO_2$/$TiO_2$ double shells. As shown in **Fig. S5,** the 1D Au@$SnO_2$@TNS hetero-nanotubes showed relatively smaller diameters compared to the single shell nanotubes (e.g., Au@TNS). This decrease in size resulted in a small improvement in the light scattering ability, as shown in **Fig. S6a**. However, the insertion of the thin $SnO_2$ layer, with higher electron mobility, led to an enhancement in the $J_{sc}$, $V_{oc}$, and FF compared to the OM-T film. Therefore, the overall conversion efficiency of the double shell-based cell was slightly higher than that of the single shell-based cell (**Fig. S6b,c**).

**Table 1**. Surface area ($S_{BET}$) and pore diameter of the maximum ($d_{p,peak}$) of various photoanodes and the photovoltaic properties of

ssDSSCs fabricated with various photoanodes at 100 mW $cm^{-2}$. PEBII was used as a solid electrolyte.

| Photoanode* | $S_{BET}$ ($m^2$/g) | $V_{oc}$ (V) | $J_{sc}$ (mA/ $cm^2$) | FF | η (%) |
|---|---|---|---|---|---|
| Dyesol | - | 0.73 | 11.0 | 0.50 | 4.0 |
| OM-T | 82.2 | 0.75 | 13.7 | 0.58 | 6.0 |
| OM-T / TNS 20% | 116.0 | 0.76 | 15.0 | 0.56 | 6.4 |
| OM-T / Au1@TNS 20% | 120.4 | 0.75 | 17.5 | 0.55 | 7.2 |
| OM-T / Au2@TNS 20% | 119.7 | 0.76 | 18.9 | 0.56 | 8.0 |
| OM-T / Au3@TNS 20% | 120.4 | 0.76 | 18.3 | 0.56 | 7.8 |
| OM-T / Au2@TNS 10% | 98.0 | 0.75 | 15.9 | 0.58 | 6.9 |
| OM-T / Au2@TNS 15% | 111.0 | 0.75 | 18.4 | 0.57 | 7.8 |
| OM-T / Au2@TNS 30% | 139.7 | 0.76 | 16.6 | 0.56 | 7.0 |
| OM-T / $SnO_2$@TNS 20% | - | 0.78 | 14.2 | 0.61 | 6.8 |
| OM-T / Au@$SnO_2$@TNS 10% | - | 0.78 | 16.7 | 0.59 | 7.6 |
| OM-T / Au@$SnO_2$@TNS 20% | - | 0.77 | 18.3 | 0.60 | 8.4 |
| OM-T / Au@$SnO_2$@TNS 30% | - | 0.78 | 16.1 | 0.56 | 7.0 |

* Dyesol: commercially available Dyesol paste (18NR-T); OM-T: organized mesoporous $TiO_2$ film prepared with a PVC-g-POEM graft copolymer as a template; Au1@TNS, Au2@TNS, and Au3@TNS: synthesized using the weight ratios of Au to Te@CNF = 2, 5, and 10%, respectively, followed by deposition of $TiO_2$ nanosheets (TNSs) and selective removal of CNF; and $SnO_2$@TNS and Au@$SnO_2$@TNS: prepared by coating $SnO_2$ on CNF, depositing TNS, and selectively removing CNF.

In order to verify the origin of the performance enhancement (especially the $J_{sc}$ enhancement of the hetero-nanotube cells), the IPCE spectra of ssDSSCs with various photoanodes were measured (**Fig. 5b**). The addition of multi-functional Au@TNS resulted in an improvement in IPCE values compared to the bare OM-T cell due to the enhancement of the light scattering, surface area, and electron transport. The DSSC fabricated with 1D TNSs with a plasmonic core showed greater IPCE values over the entire wavelength range, which is attributed to the plasmon resonance effect. This trend is similar to the J-V measurement results mentioned above. When calculating the IPCE enhancement ratio caused by the addition of plasmonic 1D TNSs (with the IPCE values of OM-T, as seen in **Fig. S7**), it is found that the enhancement is significant. Two new peaks are observed; the peak between 450 and 480 nm is likely due to plasmon-assisted, enhanced light absorption and the peak between 730 and 750 nm is likely caused by the strong light scattering of the tubular structure and plasmon resonance effects.[17] In our structure, gold nanoparticles are decorated inside the $TiO_2$ nanotubes; this very small distance between the gold nanoparticles and the dye molecules, without any protection shell, can generate strong localized surface plasmon resonance, resulting in an enhancement in the near-field effects and absorption of dye molecules surrounding the gold nanoparticles.

In terms of the plasmon-induced enhancement in the electrochemical properties, it has been reported that one of the main advantages is the promotion of interfacial carrier separation due to the electromagnetic field generated near plasmonic particles. Furthermore, in our case, the aligned, inner-decoration of gold nanoparticles along the one-dimensional nanostructure can contribute to enhanced electron transport and suppressed electron recombination, which lead to enhanced electron collection.[50,51] To further investigate the synergetic effect of 1D nanostructures and plasmonic nanoparticles on the electrochemical properties, IMPS/IMVS measurements were performed for ssDSSCs fabricated with various photoanodes, as shown in **Fig. 6-7**. This data shows that the incorporation of 1D TNSs resulted in a significant enhancement in the diffusion coefficient, electron lifetime, and diffusion length compared to the OM-T cell. These improvements were due to the 1D nanostructure, which helped promote electron transport. Interestingly, the incorporation of the aligned gold cores inside the 1D nanotubes can further increase electron transport and reduce electron recombination. This is probably due to the fact that the aligned gold nanoparticles along the 1D nanostructure offer uniformly positioned active sites that offer 'hot electrons' through surface plasmon resonance.

## Experimental details

### Materials

Poly(vinyl chloride) (PVC, $M_n$ = 55,000 g $mol^{-1}$), poly(oxyethylene methacrylate) (POEM, poly(ethylene glycol) methyl ether methacrylate, $M_n$ = 475 g $mol^{-1}$), 1,1,4,7,10,10-hexamethyltriethylene tetramine (HMTETA, 99%), copper(I) chloride (CuCl, 99%), titanium(IV) isopropoxide (TTIP, 97%), a hydrogen chloride solution (HCl, 37 wt%), chloroplatinic acid hexahydrate ($H_2PtCl_6$), tellurium dioxide($TeO_2$, 99.995%), poly(vinyl pyrrolidone) (PVP, $M_w$ = 55,000 g $mol^{-1}$), sodium hydroxide (NaOH, 97%), D-(+)-glucose (99.5%), gold(III) chloride hydrate ($HAuCl_4$, 99.999%), mercapto-acetic acid (98%), tin(II) chloride dihydrate (98%), urea (99%), and diethylenetriamine (99%) were purchased from Sigma-Aldrich. Tetrahydrofuran (THF), *N*-methyl pyrrolidone (NMP), 2-propanol, chloroform, and acetonitrile were purchased from J. T. Baker. Deionized water (>18 MΩm) was obtained with a water purification system made by Millipore Corporation. Ruthenium dye (535-bisTBA, N719) was purchased from Solaronix, Switzerland. Fluorine-doped tin oxide (FTO) conducting glass substrates (TEC8, 8 ohms $sq^{-1}$, 2.3 mm thick) were purchased from Pilkington, France. All solvents and chemical reagents used in the experiments were obtained from commercial sources as guaranteed grade reagents and used without further purification.

### Preparation of Te@CNF

Ultra-long tellurium nanowires with a few nm diameters were synthesized through a hydrothermal reaction after the modification of a previously reported method.[41,42] Briefly, 0.12 g of $TeO_2$ powder, 0.6 g of PVP, and various amounts of NaOH (0.4, 0.8, 1.2 g) are dissolved into 48 mL of ethylene glycol by heating to form a clear solution. Tellurium nanowires were obtained after a hydrothermal reaction at 180 °C for 3 h. An excess amount of acetone was added into 10 mL of the prepared tellurium nanowires solution. The precipitated blue-black tellurium nanowires were collected by centrifuging at 6000 rpm for 10 min, re-dispersed into 80 mL of a glucose solution containing 5 g of glucose, and exposed to a hydrothermal reaction at 160 °C for different reaction times of 18, 36, and 48 h.

Products were filtered and washed with ethanol and DI water several times and dried in the vacuum oven overnight.

**Preparation of Au@CNF**

Au@CNF was prepared by a galvanic replacement reaction, from tellurium to gold, using Te@CNF as the template. 3 g of vacuum-dried Te@CNF-100 were re-dispersed in DI water to form a brown, wool-like, homogeneous solution. Different amounts of the gold precursor ($HAuCl_4$) were added to the aforementioned homogeneous solution with 2, 5, and 10 weight ratios of gold to Te@CNF (noted as Au1@CNF, Au2@CNF, and Au3@CNF, respectively), and stirred at 50 $^oC$ for 12 h. To prepare pure CNF, the tellurium core was removed by immersion in an acid $H_2O_2$ solution ($HCl : H_2O_2 : H_2O = 2 : 5 : 23$, v/v) at room temperature for 12 h. After either the etching or galvanic replacement reactions, the samples were filtrated and washed. In the case of Te@CNF-50, 10 wt% of $HAuCl_4$ was added to the Te@CNF solution. Similar steps were repeated to prepare Au@CNF-50.

**Preparation of Au@TNS**

0.1 g of pure CNF and Au@CNF with different amounts of gold cores were re-dispersed into a 40 mL IPA, 0.3 mL DETA, and 0.3 mL TTIP solution by sonication and magnetic stirring. Homogeneous solutions were transferred to 100 mL Teflon-lined autoclaves, heated to 200 ℃, and maintained for 24 h. After the reaction, the autoclave was cooled to room temperature and the products were collected by filtration and washed with ethanol and DI water.

**Preparation of Au@$SnO_2$@TNS hetero-nanotubes**

0.1 g of pure CNF and Au@CNF-50 were re-dispersed into 40 mL of a 20 mM mercapto solution. 0.1 g of $SnCl_2$, 0.5 g of urea, and 0.5 mL of hydrochloric acid were added to the solution. This was heated to 80 $^oC$ in an oil bath and stirred for 6 h. After reaction, the product was collected by filtration and washed with ethanol and DI water. For the deposition of TNSs, the same hydrothermal reaction was repeated.

**Preparation of plasmonic, inner-decorated photoanodes**

First**,** FTO-coated conductive glass substrates were cleaned in a series of isopropanol, chloroform, and isopropanol by ultrasonication for 30 min. After cleaning, a titanium(IV) bis(ethyl acetoacetato)diisopropoxide solution in butanol was spin-coated onto the FTO glass followed by annealing at 450 $^oC$ for 30 min to form the blocking layer. The OM-T films were prepared by the addition of preformed $TiO_2$ nanocrystals to a premixed, 2 mL solution of 10 wt% PVC-g-POEM, which was used as the structure directing agent.[36-39] Briefly, 0.2 g of the PVC-*g*-POEM graft copolymer was added to tetrahydrofuran and stirred overnight. This was followed by the addition of 0.35 g of preformed $TiO_2$ nanocrystals. Finally, 0.15 mL of a mixture of $HCl/H_2O$ (37:63 weight ratio) was added to the solution to induce self-assembly and increase the dispersion of the mixture. The viscous mixtures were deposited onto FTO glass using a doctor-blade technique, followed by sintering at 450 $^oC$ for 30 min. In the case of the composite films, the 1D TNSs and $SnO_2$@TNS with and without plasmonic Au cores were dispersed in 2 mL of a 10 wt% PVC-g-POEM solution by ultrasonication for 30 min. The same procedure was repeated for OM-T-based composite photoanodes.

**Fabrication of ssDSSCs**

The ssDSSCs were fabricated by drop-casting the polymer electrolyte solution onto the photoanode and then covering this with the counter electrode, as described in a previously reported procedure.[36-39] The prepared photoanodes were immersed in an N719 dye solution (0.5 mM in ethanol) for 24 h at room temperature and then washed with ethanol. PEBII ($M_w$ = 15,000 g/mol), which is a solid, rubbery polymer, was synthesized via free radical polymerization and used as the solid electrolyte.[36-39] The Pt counter electrodes were prepared by spin-coating a 1 wt% $H_2PtCl_6$ solution in isopropanol onto the FTO glass and then sintering at 450 $^oC$ for 30 min. The PEBII solution in acetonitrile was directly cast onto the photoanodes. The photoanodes and counter electrodes were then superimposed and pressed between two glass plates to achieve slow solvent evaporation and create a thin electrolyte layer. The cells were placed in a vacuum oven for one day to ensure complete solvent evaporation. The active area, determined by a black mask, was 0.16 $cm^2$.

**Characterization**

The morphology of hierarchical 1D nanotubes and their mesoporous structures were observed by a field-emission scanning electron microscope (FE-SEM, SUPRA 55VP, Carl Zeiss, Germany). Energy-filtering transmission electron microscopy (EF-TEM) images were obtained in order to investigate the presence of plasmonic nanoparticles and the inner-decoration inside the 1D structures using a Philips CM30 microscope operated at 300 kV. After drying the samples at room temperature for one day in a vacuum oven, the specific surface area and pore size distribution of the mesoporous structures with plasmonic nanocomposites were measured from a $N_2$ adsorption-desorption isotherm via Brunauer-Emmett-Teller (BET, for specific surface area) and Barrett-Joyner-Halenda (BJH, for pore size distribution) methods using a Belsorp-mini II device. The diffuse reflectance spectra of the films were acquired using a UV-visible spectrophotometer (Hewlett-Packard, Hayward, CF) over a sample area of roughly 5 $\mu m^2$ with magnification of 100. A spectral range of 300–800 nm was explored using a tungsten-halogen lamp.

The performances of DSSCs were characterized using an electrochemical workstation (Keithley Model 2400) and a solar simulator (1000 W xenon lamp, Oriel, 91193). The spectral mismatch between the simulated light and natural sunlight was corrected for with a certified reference Si solar cell (Fraunhofer Institute for Solar Energy System, Mono-Si + KG filter, Certificate No. C-ISE269) to obtain a sunlight intensity of one (100 mW $cm^{-2}$). IPCE measurement was carried out over wavelengths ranging from 300 nm to 800 nm using a 150 W Arc Xe lamp source. IMPS/IMVS measurements were performed on an electrochemical workstation equipped with a frequency response analyzer under a modulated red light emitting diode (635 nm) driven by a source supply, which provided both the DC and AC components of the illumination. The frequency range was set from 0.1 Hz to 1 MHz.

## Conclusions

In this study, plasmonic gold nanoparticles were successfully decorated on the interior of hierarchical 1D hetero-nanotubes with single or double shell metal oxide nanotubes using a 1D Te/CNF nanostructure as a dual template and a galvanic exchange reaction. The inner-decoration of gold nanoparticles can generate a synergetic effect between the plasmonic properties and the structural advantages of hierarchical 1D TNSs, simultaneously creating a larger surface area, excellent electron transport, and improved light scattering abilities, which prevents the exposure of the plasmonic cores to the electrolyte. In the presence of gold cores in hetero-nanotube photoanodes, the plasmonic nanoparticles promoted charge transfer and electron transport as well as plasmon-assisted light harvesting, which were attributed to the localized surface plasmon resonance and the presence of an electromagnetic field. The plasmonic 1D TNSs or double shell $SnO_2$@TNS-containing gold nanoparticles were incorporated into organized mesoporous $TiO_2$ films with large pores, high porosity, and good interconnectivity. As a result, the highest efficiencies of 8.0% and 8.4% were obtained for 1D Au@TNS single shell and Au@$SnO_2$@TNS double shell-based ssDSSCs, respectively, representing some of the greatest values for N719-based ssDSSCs. The improved DSSC performance was attributed to good pore-filling for solid electrolytes, faster electron transfer, and enhanced light scattering, as revealed by diffuse reflectance, J-V curves, IPCE analysis, and IMPS/IMVS measurements.

## Acknowledgements

We acknowledge the financial support of the National Research Foundation (NRF) grant funded by the Center for Advanced Meta-Materials (CAMM) (2014M3A6B3063716), the Active Polymer Center for Pattern Integration (2007-0056091) and the Korea Center for Artificial Photosynthesis (KCAP) (2009-0093883).

## Notes and references

Department of Chemical and Biomolecular Engineering, Yonsei University, 262 Seongsanno, Seodaemun-gu, Seoul 120-749, South Korea , E-mail: *jonghak@yonsei.ac.kr*

† Electronic Supplementary Information (ESI) available: [details of any supplementary information available should be included here]. See DOI: 10.1039/b000000x/

‡ Footnotes should appear here.

1. B. Oregan and M. Gratzel, *Nature*, 1991, **353**, 737-740.
2. L. Yang and W. W.-F. Leung, *Adv. Mater.*, 2013, **25**, 1792-1795.
3. R. Casillas, F. Lodermeyer, R. D. Costa, M. Prato and D. M. Guldi, *Adv. Energy Mater.*, 2014, **4**, 1301577.
4. X. Fang, Z. Yang, L. Qiu, H. Sun, S. Pan, J. Deng, Y. Luo and H. Peng, *Adv. Mater.*, 2014, **26**, 1791-1791.
5. X. Wu, G. Q. Lu and L. Wang, *Adv. Energy Mater.*, 2013, **3**, 703-703.
6. T. Leijtens, I. K. Ding, T. Giovenzana, J. T. Bloking, M. D. McGehee and A. Sellinger, *ACS Nano*, 2012, **6**, 1455-1462.
7. S. Nejati and K. K. S. Lau, *Nano Lett.*, 2010, **11**, 419-423.
8. H. Wang, J. Li, F. Gong, G. Zhou and Z.-S. Wang, *J. Am. Chem. Soc.*, 2013, **135**, 12627-12633.
9. H. Wang, X. Zhang, F. Gong, G. Zhou and Z.-S. Wang, *Adv. Mater.*, 2012, **24**, 121-124.
10. C. Xu, J. Wu, U. V. Desai and D. Gao, *Nano Lett.*, 2012, **12**, 2420-2424.
11. F. Lodermeyer, R. D. Costa, R. Casillas, F. T. U. Kohler, P. Wasserscheid, M. Prato and D. M. Guldi, *Energy Environ. Sci.*, 2015.
12. M. Z. Liu, M. B. Johnston and H. J. Snaith, *Nature*, 2013, **501**, 395-398.
13. F. Sauvage, D. H. Chen, P. Comte, F. Z. Huang, L. P. Heiniger, Y. B. Cheng, R. A. Caruso and M. Graetzel, *ACS Nano*, 2010, **4**, 4420-4425.
14. Y. H. Jang, Y. J. Jang, S. T. Kochuveedu, M. Byun, Z. Q. Lin and D. H. Kim, *Nanoscale*, 2014, **6**, 1823-1832.
15. J. B. Joo, M. Dahl, N. Li, F. Zaera and Y. D. Yin, *Energy Environ. Sci.*, 2013, **6**, 2082-2092.
16. W. Zhang, M. Saliba, S. D. Stranks, Y. Sun, X. Shi, U. Wiesner and H. J. Snaith, *Nano Lett.*, 2013, **13**, 4505-4510.
17. Y. Li, H. Wang, Q. Feng, G. Zhou and Z.-S. Wang, *Energy Environ. Sci.*, 2013, **6**, 2156-2165.
18. L. L. Liang, Y. M. Liu, C. H. Bu, K. M. Guo, W. W. Sun, N. Huang, T. Peng, B. Sebo, M. M. Pan, W. Liu, S. S. Guo and X. Z. Zhao, *Adv. Mater.*, 2013, **25**, 2174-2180.
19. Y. Li, G. F. Wang, K. Pan, B. J. Jiang, C. G. Tian, W. Zhou and H. G. Fu, *J. Mater. Chem.*, 2012, **22**, 20381-20386.
20. W. Q. Zou, C. Visser, J. A. Maduro, M. S. Pshenichnikov and J. C. Hummelen, *Nat. Photonics*, 2012, **6**, 560-564.
21. S. Y. Heo, J. K. Koh, G. Kang, S. H. Ahn, W. S. Chi, K. Kim and J. H. Kim, *Adv. Energy Mater.*, 2014, **4**, 1300632.
22. S. Wooh, H. Yoon, J.-H. Jung, Y.-G. Lee, J. H. Koh, B. Lee, Y. S. Kang and K. Char, *Adv. Mater.*, 2013, **25**, 3111-3116.
23. J. Kim, J. K. Koh, B. Kim, J. H. Kim and E. Kim, *Angew. Chem.-Int. Edit.*, 2012, **51**, 6864-6869.
24. D. J. Kim, J. K. Koh, C. S. Lee, J. H. Kim, *Adv. Energy Mater.*, 2014, **4**, 1400414.
25. C. Lopez-Lopez, S. Colodrero, M. E. Calvo and H. Miguez, *Energy Environ. Sci.*, 2013, **6**, 1260-1266.
26. M. Guo, K. Y. Xie, J. Lin, Z. H. Yong, C. T. Yip, L. M. Zhou, Y. Wang and H. T. Huang, *Energy Environ. Sci.*, 2012, **5**, 9881-9888.
27. S. Colodrero, A. Forneli, C. Lopez-Lopez, L. Pelleja, H. Miguez and E. Palomares, *Adv. Funct. Mater.*, 2012, **22**, 1303-1310.
28. S. Guldin, M. Kolle, M. Stefik, R. Langford, D. Eder, U. Wiesner and U. Steiner, *Adv. Mater.*, 2011, **23**, 3664-3668.
29. J. T. Park, J. H. Prosser, D. J. Kim, J. H. Kim and D. Lee, *ChemSusChem*, 2013, **6**, 856-864.
30. J. T. Park, J. H. Prosser, S. H. Ahn, S. J. Kim, J. H. Kim and D. Lee, *Adv. Funct. Mater.*, 2013, **23**, 2193-2200.
31. R. A. Naphade, M. Tathavadekar, J. P. Jog, S. Agarkar and S. Ogale, *J. Mater. Chem. A*, 2014, **2**, 975-984.
32. H. Choi, W. T. Chen and P. V. Kamat, *ACS Nano*, 2012, **6**, 4418-4427.
33. W. L. Liu, F. C. Lin, Y. C. Yang, C. H. Huang, S. Gwo, M. H. Huang and J. S. Huang, *Nanoscale*, 2013, **5**, 7953-7962.
34. S. W. Sheehan, H. Noh, G. W. Brudvig, H. Cao and C. A. Schmuttenmaer, *J. Phys. Chem. C*, 2013, **117**, 927-934.
35. J. Qi, X. Dang, P. T. Hammond and A. M. Belcher, *ACS Nano*, 2011, **5**, 7108-7116.
36. S. H. Ahn, W. S. Chi, J. T. Park, J. K. Koh, D. K. Roh and J. H. Kim, *Adv. Mater.*, 2012, **24**, 519-522.
37. S. H. Ahn, W. S. Chi, D. J. Kim, S. Y. Heo and J. H. Kim, *Adv. Funct. Mater.*, 2013, **23**, 3901-3908.
38. S. H. Ahn, D. J. Kim, W. S. Chi and J. H. Kim, *Adv. Funct. Mater.*, 2014, **24**, 5037-5044.
39. S. H. Ahn, D. J. Kim, W. S. Chi and J. H. Kim, *Adv. Mater.*, 2013, **25**, 4893-4897.
40. H.-W. Liang, L. Wang, P.-Y. Chen, H.-T. Lin, L.-F. Chen, D. He and S.-H. Yu, *Adv. Mater.*, 2010, **22**, 4691-4695.
41. H. W. Liang, Q. F. Guan, L. F. Chen, Z. Zhu, W. J. Zhang and S. H. Yu, *Angew. Chem.-Int. Edit.*, 2012, **51**, 5101-5105.
42. X. H. Xia, Y. Wang, A. Ruditskiy and Y. N. Xia, *Adv. Mater.*, 2013, **25**, 6313-6333.
43. H. W. Liang, W. J. Zhang, Y. N. Ma, X. Cao, Q. F. Guan, W. P. Xu and S. H. Yu, *ACS Nano*, 2011, **5**, 8148-8161.
44. G. Q. Zhang and X. W. Lou, *Sci. Rep.*, 2013, **3,** 1470.
45. J. Yu, J. Fan and K. Lv, *Nanoscale*, 2010, **2**, 2144-2149.
46. L. Sun, Y. Huang, Md. A. Hossain, K. Li, S. Adams, Q. Wang, *J. Electrochem. Soc.* 2012, **159**, D323-D327.

47. X. Wu, Z. Chen, G. Q. Lu and L. Wang, *Adv. Funct. Mater.*, 2011, **21**, 4167-4172.
48. P. Reineck, G. P. Lee, D. Brick, M. Karg, P. Mulvaney and U. Bach, *Adv. Mater.*, 2012, **24**, 4750-4755.
49. S. Chang, Q. Li, X. D. Xiao, K. Y. Wong and T. Chen, *Energy Environ. Sci.*, 2012, **5**, 9444-9448.
50. J. Choi, G. Kang, T. Park, *Chem. Mater.* 2015, **27**, 1359-1366.
51. J. Choi, S. Song, G. Kang, T. Park, *ACS Appl. Mater. Interfaces* 2014, **6**, 15388-15394.

# Graphical Abstract

**One-dimensional, hierarchical, hetero-nanotube photoanodes**, consisting of Au cores and $SnO_2/TiO_2$ nanosheet double shells, were prepared to provide a large surface area, excellent electron transport, and improved light scattering. The resulting solid-state dye-sensitized solar cells showed enhanced efficiency up to 8.4% at 100 mW $cm^{-2}$, one of the highest values observed for N719 dye.